Dynamic Blood Flow and Wall Shear Stress in Pulmonary Hypertensive Disease

Arthur Postles[1], Alys R. Clark[1] and Merryn H. Tawhai[1]

Abstract— **This study provides new model of pulsatile flow in the pulmonary circulation in health and pulmonary hypertensive disease. Structural vascular remodeling typical of pulmonary hypertensive disease was implemented in the model by progressively altering the mechanical properties of the arterial geometry and progressively increasing the inlet pulse pressure (PP). The transmission of PP throughout the tree was shown to increase in advanced stages of disease, creating the potential for a 'vicious-cycle' of damage to vasculature. Wall shear stress (WSS) was shown to be highest in the terminal arteries of the model and increased significantly with disease. A further trend observed in WSS results was that high WSS values began to 'climb' the arterial tree towards the proximal vessels as disease progressed. This suggests a link between WSS and distal remodeling in pulmonary hypertensive disease, which initiates in the small muscular arteries and arterioles and spreads into larger arteries as the disease progresses.**

I. INTRODUCTION

Pulmonary hypertension (PH) is a debilitating condition that is indicated by an increase in pulmonary artery pressure from its normal mean value of 15 mmHg to greater than 25 mmHg at rest. PH has a range of contributing factors, including genetics, acute occlusion of pulmonary blood vessels, and chronic lung disease. Blood vessel remodeling is accepted to be a common feature of all types of PH [1]. Common to most types of PH are a thickening of the medial and intimal layers of the vessel wall, which can then progress to complete occlusion of small arteries, fibrosis and lesions [1], [2]. Wall shear stress (WSS) is thought to maintain equilibrium in the pulmonary vasculature [3]. The endothelial cells that are in contact with blood constantly receive information about the state of flow via WSS and the flow information is transmitted to the smooth muscle cell (SMC) layer in muscular arteries, triggering vasoconstriction or vasodilation to maintain baseline WSS values [3]. Chronic changes to the pulmonary flow are theorized to chronically alter the vasoregulatory states, eventually leading to structural remodeling of the blood vessels [3].

The progressive changes in vascular structure with remodeling have been described in detail for idiopathic pulmonary hypertension (IPAH) [4]. These structural changes are common to other forms of PH. including Chronic Thromboembolic Pulmonary Hypertension (CTEPH) - a deadly disease of the pulmonary vasculature that develops from episodes of unresolved pulmonary embolism (PE) [5]. Untreated, the course of progressive remodeling causes increasing hypertension that eventually causes heart failure. Treatment of PH depends on the stage of disease progression, however, progression of remodeling - such as that described by Heath and Edwards [4] - is based on histology and is not well predicted by current diagnostic procedures [6]. Understanding how the stage of remodeling relates to integrated measurements of pulmonary hemodynamics offers a potential strategy for stratifying patients to optimize treatment in PH. In this study we present a pulsatile blood flow model in pulmonary artery geometries to investigate the nature of transient pressure, flow and WSS in health and disease. This model incorporates the structural changes in the pulmonary vasculature as described by Heath and Edwards [4].

[1]All authors are with the Auckland Bioengineering Institute, University of Auckland, New Zealand. Corresponding author A. R. Clark alys.clark@auckland.ac.nz

II. METHODS

An anatomically-based pulmonary artery geometry was created for a single subject using subject-specific lung modeling techniques developed and described previously [7]. The geometries consist of one-dimensional, spatially distributed elements that represent the anatomical branching structure of the human lung. To date, simulations of perfusion in anatomically-based geometries such as this have been solved in the steady-state [7]. The steady-state model assumes a constant flow or pressure inlet boundary condition (BC) with the pressure at the outlet of the pulmonary veins into the left atrium constituting the outlet BC. These BCs, whether pressure or flow, can be obtained from diagnostic procedures such as an echocardiogram or cardiac catheterization.

Wave Propagation Model. A wave propagation model - based on that of Duan and Zamir [8], [9], [10] - was implemented within the anatomically based geometry. Each element (vessel segment) in the vascular geometry connects upstream and downstream local nodes that are part of the global node network of the tree. Vessel segment length was calculated for every segment, and a radius was assigned based on the vessel order. For all elements except the terminal elements, the defined data allowed calculation of a characteristic admittance, effective admittance, and reflection coefficient. These properties are defined in Equations 1, 3 and 5.

Characteristic admittance is the inverse of impedance and depends on the physical properties of a single vessel element and the fluid. For a single vessel element,

$$Y_v = \left(\frac{A}{\rho c_v}\right) \times \sqrt{\epsilon_r}, \tag{1}$$

where A is cross sectional area defined from the vessel geometry, ρ is the fluid density, defined in Table I, and the viscous term ϵ_r is defined in reference [9]. Viscous

978-1-4244-7929-0/14/$26.00 ©2014 IEEE

wavespeed, c_v, is given by,

$$c_v = \sqrt{\frac{1}{2\rho\alpha}} \times \sqrt{\epsilon_r}, \tag{2}$$

where α is blood vessel compliance given in Table I. Effective admittance is defined as

$$Y_e = Y_v \left(\frac{(Y_1 + Y_2) + iY_0 tan\theta}{Y_v + i(Y_1 + Y_2) tan\theta} \right). \tag{3}$$

Characteristic admittance, Y_v, was then known and the tree connectivity was used to define effective admittances of the two daughter elements, Y_1 and Y_2. The variable θ, defined as,

$$\theta = \frac{\omega l}{c_v}, \tag{4}$$

where wavespeed, c_v, is already defined, l is vessel length which is part of the geometry specification, and ω is the frequency of the input waveform in rads^{-1}. Finally, the reflection coefficient, R, is

$$R = \frac{Y_v - (Y_1 + Y_2)}{Y_v + (Y_1 + Y_2)}. \tag{5}$$

TABLE I: The physical constants used to predict blood flow in the model.

Constant	Value	Source
Blood density, ρ	1.06 $\times 10^3$ kgm^3	[11]
Blood viscosity, μ	3.5 $\times 10^{-3}$ Pa·s	[11]
Artery Compliance, α	0.02 mmHg^{-1}	[12]

Outlet Boundary Conditions. The terminal elements represent the arteries that feed the acini of the lung (vessels that accompany terminal bronchioles of the airway tree) [7]. BCs defining the reflection coefficient, R, and the effective admittance, Y_e, are the BCs required for each terminal element in the vascular mesh. The values chosen for these BCs are important as they represent the sum of the pulmonary vascular resistance distal to the terminal arteries tha are included in the model. To find a reasonable estimate for acinar resistance, the admittance Equations 1 to 5 were applied to an acinar geometry that has been described previously [7]. The geometry consists of nine symmetrically bifurcating generations of arterioles and a mirroring set of venules. Each arteriole element is connected to its mirroring venule by a capillary sheet and the terminal arterioles are connected to the terminal venules at their ends by capillary sheets. The radius and length of each arteriole generation decreases from the radius and length of the artery that feeds the acinus down to typical pre-capillary vessel dimensions (radius: 10 μm, length: 130 μm). The viscosity of blood also varies within these microvessels as a function of hematocrit and is assumed to range from 4×10^{-3} Pa·s to 1.92×10^{-3} Pa·s corresponding to a decrease in hematocrit from 45% to 30% [13].

This defines all the data required to solve the admittance system of equations 1 to 5, except for capillary radius and the downstream admittances at the boundary of the model. The boundary for this acinar resistance model was set in the venules into which the capillaries drain. The entire venule tree was not included as it was assumed that venules and veins contribute a negligible amount to pulmonary vascular resistance. In the boundary venules, the reflection coefficient was set equal to zero and the effective admittance assumed to be equal to characteristic admittance.

To determine the capillary dimensions we considered the capillary as two sheets separated by posts [7]. The capillary opening was assumed to be rectangular allowing an hydraulic diameter to be calculated for the rectangular opening. The hydraulic diameter for a rectangular duct is given by,

$$D_e = \frac{2ab}{a+b}, \tag{6}$$

where a and b are the two sides of the rectangle. The assumption that hydraulic diameter is equivalent to capillary diameter can potentially have a significant effect on the assumed resistance of the capillaries. With the blood vessels modeled in a healthy state, this assumption produced a pulse pressure (PP) in the terminal arteries that was 0.28 the magnitude of the inlet PP. The terminal to inlet PP ratio is expected to be in the region of 0.3 [14] so the model compares well to data in this respect.

Inlet Boundary Conditions. A pulsatile pressure wave form was prescribed at the inlet vessel (the main pulmonary artery). An array of discrete data points was created from a generic waveform [15]. A Fourier decomposition was then performed on the discrete input pressure data to produce an oscillatory waveform.

Pressure and Flow. With inlet pressure defined, pressure and flow can be predicted in each vessel element,

$$p(x,t) = p_0 e^{i\omega\left(t - \frac{x}{c_v}\right)} + R p_0 e^{i\omega\left(t + \frac{x}{c_v} - 2i\omega l\right)}, \tag{7}$$

$$q(x,t) = \left(\frac{A}{\rho c_v}\right) p_0 e^{i\omega\left(t - \frac{x}{c_v}\right)} - \left(\frac{A}{\rho c_v}\right) R p_0 e^{i\omega\left(t + \frac{x}{c_v} - \frac{2l}{c_v}\right)}. \tag{8}$$

The amplitude of the pressure wave, p_0, is defined by a continuity condition. The continuity condition is found by evaluating Equation 7 at the node connecting two elements. In the upstream element $x = L$ (where L is the element length) and in the downstream element $x = 0$. Equating the results gives the downstream element pressure amplitude, $p_{0,down}$, in terms of the upstream element pressure amplitude, $p_{0,up}$ [8]. This results in

$$p_{0,down} = p_{0,up} \frac{(1 + R_{up}) e^{\frac{-i\omega l_{up}}{c_{v,up}}}}{1 + R_{down} e^{\frac{-2i\omega l_{down}}{c_{v,down}}}}. \tag{9}$$

The flow continuity condition follows from Equation 8

$$q_{0,down} = \left(\frac{A}{\rho c_v}\right) p_{0,down}. \tag{10}$$

Equation 7 can be used to calculate the pressure amplitude in the inlet element from the pressure amplitude at the inlet. After this, a similar process is followed to that used

for admittance, this time stepping down the tree. WSS is defined as in [16]. The model algorthithm was implemented in Matlab (2012a, The Mathworks Inc) to calculate the maximum amplitude in each element takes approximately 3 min and a complete simulation takes 31 min on a desktop PC with a 2.4GHz processor and 12GB RAM.

Remodeling. Structural changes to arteries were implemented with reference to a description of vascular remodeling in Idiopathic Pulmonary Hypertension (IPAH) [4]. The structural changes implemented were applied uniformly throughout the arterial geometry over eight steps of remodeling. Thickening of the media due to *medial hypertrophy and hyperplasia* of smooth muscle cells was modeled as a decrease in vascular compliance of the muscular arteries. To implement this an element specific compliance array was defined. At a given remodeling step, the muscular artery elements, with diameter 1000 μm to 100 μm, were assigned a decreased compliance. The compliance ranged from α at step 1 to $\frac{1}{6}\alpha$ at step 8 (α in Table I). The *proliferation of endothelial cells* was modeled by uniformly reducing the radius of vessel elements within a separate set of diameter limits. At step 8, vessels with diameter 500 μm to 30 μm were narrowed to 0.55 of their original radius. *Pruning* is the complete occlusion of small arteries due to *progressive proliferation* and was modeled by specifying a fraction of vessels within specified diameter limits and reducing the vessel diameters to effectively zero. In the healthy state of step 1 no pruning was implemented, while at step 8 43.75% of extra-acinar vessels with diameter less than 500 μm were pruned. *Fibrosis* refers to an increase in stiff, extracellular materials such as collagen in the vessel wall and is modeled by a decrease in vessel compliance. The compliance of vessels with diameter 500 μm to 30 μm was reduced to $\frac{1}{2}\alpha$ at step 8. At step 1 the inlet waveform PP was set to a healthy value of 11 mmHg and this value was increased to 36 mmHg at step 8 - based on hemodynamic data.

III. RESULTS

Figure 1 plots two sets of mean, normalized, terminal pulse pressure (PP) results against progressive remodeling steps. The results marked by circles are normalized to a constant healthy inlet PP of 11 mmHg. These results show a substantial increase in PP caused by remodeling throughout the pulmonary artery model. The greatest increases are shown to occur after step 4. The results marked by crosses in Figure 1 are PPs normalized to the inlet PP result of the same simulation. These results then illustrate the fraction of the inlet PP that reaches the terminal arteries. The data show that in advanced remodeling stages, a greater fraction of the inlet PP reaches the terminal arteries. As with the other PP results, the more substantial changes occur after step 4 of remodeling. The PP results (normalized with respect to the inlet PP of the same simulation) are shown throughout the entire pulmonary artery mesh of the subject in Figure 2. In this Figure, the mesh on the left displays step 1 results and the mesh on the right step 8 results. The distribution of color shows the increased fraction of inlet PP that reaches the terminals with advanced remodeling.

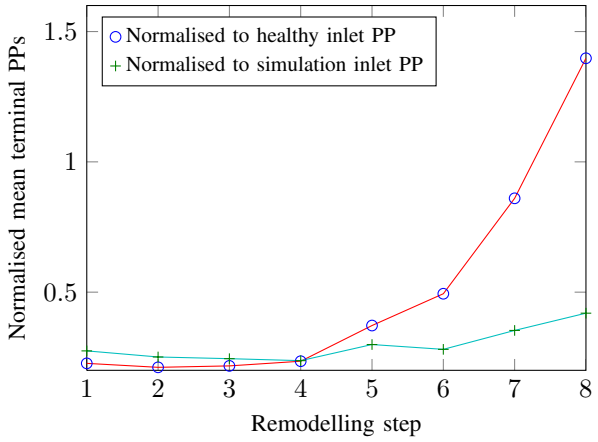

Fig. 1: Mean terminal normalized PP results against progressive remodeling steps. The results marked by circles are normalized to a constant healthy inlet PP of 11 mmHg and show the substantial increase in PP caused by remodeling throughout the pulmonary arteries. The results marked by crosses are normalized to the inlet PP result of the same simulation and show that in advanced remodeling stages, a greater fraction of the inlet PP reaches the terminals.

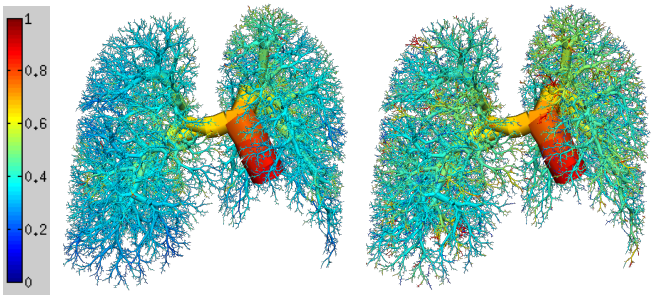

Fig. 2: PP results normalized to the same simulation inlet PP are visualized here on the pulmonary artery mesh. The mesh on the left displays step 1 results and the mesh on the right step 8 results. The distribution of color shows the increased fraction of inlet PP that reaches the terminals with advanced remodeling.

Figure 3 plots the mean WSS in the terminal arteries against progressive remodeling. WSS is shown to increase reasonably consistently over each remodeling step, from 1.91 Pa at step 1 to 16.27 Pa at step 8. WSS throughout the pulmonary arteries is visualized in Figure 4 for step 1 on the left and step 8 on the right. The color spectrum shows that WSS in the distal arteries reaches much higher values at advanced stages of remodeling.

IV. DISCUSSION

The increase in inlet pressure amplitude had the expected effect of causing increased pressure amplitudes throughout the pulmonary vasculature. Normalized PP increased throughout the vasculature in the case of severe remodeling. Increases in the normalized data suggest that the structural changes to the arterial geometry result in less attenuation

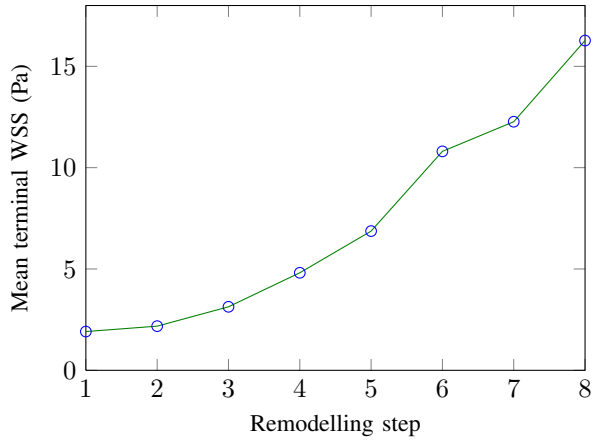

Fig. 3: Mean WSS in the terminal arteries against progressive remodeling. WSS is shown to increase with each step of remodeling and to eventually reach markedly raised levels.

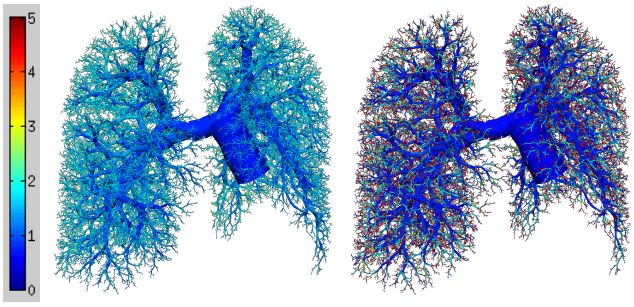

Fig. 4: WSS through the pulmonary arteries are visualized here for step 1 on the left and step 8 on the right. The color spectrum shows that WSS in the distal arteries reaches much higher values at advanced stages of remodeling.

of the pressure wave as it travels through the arterial tree. As well as increased inlet PP, an increased proportion of the inlet PP reaches the terminal arteries. This trend suggests a circular cycle of chronic remodeling where initial pressure increases in the perfused vascular bed are caused by the occlusion of proximal arteries, then the arteries in the perfused vascular bed undergo structural changes in response to increased pressures. In turn the structural changes cause an increase in the proportion of pressure pulse throughout the arterial tree. The increased pressure pulse contributes to further structural remodeling of the vasculature and the cycle continues on.

The shear stress results in baseline simulations showed a trend of WSS being inversely correlated with vessel diameter. WSS values in the pulmonary trunk and proximal vessels were markedly lower than WSS in the terminal arteries. The structural remodeling and increased pulse pressure introduced to simulate disease progression caused substantial WSS increases in the terminal arteries. Higher WSS values also began to 'climb' the arterial tree towards the proximal vessels.

These results certainly indicate that WSS could play a significant role in the vascular remodeling seen in IPAH and CTEPH. There is an interesting correlation between the observation that WSS is high in the terminal arteries at baseline and begins to climb the tree, and the observations of vascular remodeling made by the histological study that was used to describe remodeling [4]. The histological study describes distal structural remodeling in PH and observes that structural changes begin in terminal arteries and arterioles and slowly spread up the arterial tree with progression of disease. The current results indicate that high WSS values follow a similar trend, suggesting a link between WSS and remodeling.

Our model is consisted with expected whole lung measures of resistance to blood flow and PP damping through the arterial tree. Thorough validation of the spatial redistribution of perfusion with remodeling is more difficult to achieve. As patients with CTEPH are carefully monitored haemodynamically, this subject cohort provides a potential validation imaging and functional data in the future.

References

[1] S. S. Laurie L. A. Shimoda. Vascular remodelling in pulmonary hypertension. *Journal of Molecular Medicine*, 91:297–309, 2013.

[2] D. Heath, H. Helmholz, and H. Burchell et al. Graded pulmonary vascular changes and hemodynamic findings in cases of atrial and ventricular septal defect and patent ductus arteriosus. *Circulation*, 18(6):1155–1166, 1958.

[3] P. F. Davies. Flow-mediated endothelial mechanotransduction. *Physiological Reviews*, 75(3):519–560, Jul 1995.

[4] D. Heath and J. E. Edwards. The pathology of hypertensive pulmonary vascular disease: A description of six grades of structural changes in the pulmonary arteries with special reference to congenital cardiac septal defects. *Circulation*, 18(4):533–547, 1958.

[5] M. M. Hoeper, E. Mayer, G. Simonneau, and L. J. Rubin. Chronic thromboembolic pulmonary hypertension. *Circulation*, 113(16):2011–2020, Apr 25 2006.

[6] N. H. Kim, P. Fesler, R. N. Channick, K. U. Knowlton, O. Ben-Yehuda, S. H. Lee, R. Naeije, and L. J. Rubin. Preoperative partitioning of pulmonary vascular resistance correlates with early outcome after thromboendarterectomy for chronic thromboembolic pulmonary hypertension. *Circulation*, 109(1):18–22, Jan 6 2004.

[7] A. R. Clark, K. S. Burrowes, and M. H. Tawhai. Contribution of serial and parallel microperfusion to spatial variability in pulmonary inter- and intra-acinar blood flow. *Journal of applied physiology*, 108(5):1116–1126, May 2010.

[8] M. Zamir. *The physics of pulsatile flow*. AIP Press ; Springer, New York, 2000.

[9] M. Zamir B. Duan. Viscous damping in one-dimensional wave transmission. *The Journal of the Acoustical Society of America*, 92(6):3358–3363, 1992.

[10] B. Duan and M. Zamir. Pressure peaking in pulsatile flow through arterial tree structures. *Annals of Biomedical Engineering*, 23(6):794–803, Nov-Dec 1995.

[11] A. R. Clark, M. H. Tawhai, E. A. Hoffman, and K. S. Burrowes. The interdependent contributions of gravitational and structural features to perfusion distribution in a multiscale model of the pulmonary circulation. *Journal of applied physiology*, 110(4):943–955, Apr 2011.

[12] G. S. Krenz and C. A. Dawson. Flow and pressure distributions in vascular networks consisting of distensible vessels. *American Journal of Physiology - Heart and Circulatory Physiology*, 284(6):H2192–H2203, 2003.

[13] Y. C. Fung. *Biomechanics: Circulation*. Springer, 1996.

[14] G. de J. Lee and A. B. DuBois. Pulmonary capillary blood flow in man 12. *The Journal of Clinical Investigation*, 34(9):1380–1390, 9 1955.

[15] A. C. Burton. *Physiology and biophysics of the circulation: An introductory text*. Year Book Medical Publishers, 1965.

[16] T. G. Papaioannou and C. Stefanadis. Vascular wall shear stress: basic principles and methods. *Hellenic journal of cardiology : HJC = Hellenike kardiologike epitheorese*, 46(1):9–15, Jan-Feb 2005.